Temperature and density fluctuations in the inner Orion Nebula

W. J. Henney, C. R. O'Dell, G. J. Ferland, M. Peimbert

1. Analysis

1.1. Deriving diagnostic line ratios from WFC3 filter images

Note: this is similar to what I wrote in the the calibration draft, but specifically tailored to line ratios rather than equivalent widths. We may in the end want to move some of it back to the other paper.

The WFC3 camera is equipped with filters that effectively target important nebular diagnostic lines. Each filter, with label j, is characterized by an effective transmission profile, or throughput, T_λ^j, which gives the wavelength-dependent conversion factor between the number of photons arriving at the *HST* entrance aperture (nominal radius: 120 cm) and the number of electrons registered by the CCD, accounting for occultation by the secondary mirror, all other optical and quantum efficiencies, and the amplifier gain. The peak value of the filter transmission profile is denoted $T_{\rm m}^j$, with typical values of 0.2–0.3, and the "rectangular width" of the profile is defined as

$$W_j = (T_{\rm m}^j)^{-1} \int_0^\infty T_\lambda^j \, d\lambda \qquad [W_j] = \text{Å}. \tag{1}$$

Extensive and continuing on-orbit calibration of the filters has been carried out (Kalirai et al. 2009, 2010; Sabbi & the WFC3 Team 2013) using white dwarf standard stars. However, since these are flat featureless continuum sources, the calibration is only sensitive to the integrated filter throughput, given by the product $W_j T_{\rm m}^j$. A general increase in the integrated throughput of 10–20% with respect to pre-launch measurements was found for all filters, which was fitted by a low-order polynomial as a function of frequency. Only the broad-band and medium-band filters were used in determining the fit, but the scatter of the narrow-band filters[1] around the resulting curve is only a few percent (see Fig. 6 of Kalirai et al. 2009).

Emission lines from photoionized regions are intrinsically much narrower than even the narrowest WFC3 filters, so the transmission of such a line, with label i, is independent of W_j and depends instead solely on the throughput at the line wavelength: $T_i^j \equiv T_\lambda^j(\lambda = \lambda_i)$. The detailed shape of the throughput curves was measured pre-launch (Brown 2006), but direct on-orbit confirmation of these curves is impossible. However, by comparing WFC3 images with ground-based spectrophotometry of emission line nebulae, it is possible to test the filter calibrations for the case where emission lines are the dominant component of the spectrum in the filter bandpass. Just such a calibration is described in detail in a companion paper (Henney et al. 2014), using multiple spectrophotometric datasets of the Orion Nebula (M42) and the evolved nearby planetary nebula NGC 6720 (the Ring Nebula), and building on an earlier study in O'Dell et al. (2013). The conclusion of this study is that the nominal filter parameters (that is, the pre-launch measurements of the shape of the throughput curve T_λ^j, combined with the on-orbit re-calibration of $W_j T_{\rm m}^j$), are consistent to within ±5% with the emission line spectrophotometry for all but a handful of filters. The largest discrepancy is found for the F469N filter, which is found to have a sensitivity to the He II λ4696 line that is 35% higher than the nominal

[1] Note, however, that the quad filters were not included in these studies.

value. However, that line is absent in M42, due to the relatively low effective temperature of the ionizing star, and the filter is instead dominated by continuum and weak [Fe III] lines. In such circumstance the nominal F469N parameters are found to be accurate.

Smaller, but still significant, discrepancies are found for the F658N and FQ575N filters, which target the [N II] lines λ6583 and λ5755, respectively. *Discuss inconsistency between Ring and Orion calibration. Ring has 5755 increased by 10%. Orion has 6583 decreased by 10%. But effects on ratio are similar.*

We model the specific intensity, I_λ(in erg s^{-1} cm^{-2} sr^{-1} Å^{-1}), of a spatially resolved astrophysical source as the sum of several narrow emission lines i, each with central wavelength λ_i and wavelength-integrated intensity I_i, plus a slowly varying continuum $I^{\rm c}_\lambda$:

$$I_\lambda = I^{\rm c}_\lambda + \sum_{i=1,n} I_i\,\delta(\lambda - \lambda_i), \tag{2}$$

where δ denotes the Dirac delta function. It is convenient to define an average continuum intensity over the passband of filter j:

$$\langle \lambda I^{\rm c}_\lambda \rangle_j = \int_0^\infty \lambda I^{\rm c}_\lambda T^j_\lambda\, d\lambda \,\Big/ \int_0^\infty T^j_\lambda\, d\lambda. \tag{3}$$

The count rate (in e$^-$/s) in a single pixel of a pipeline-reduced (bias-subtracted, flat-fielded, drizzled) WFC3 image should then be

$$R_j = C_{\rm WFC3} \left(\langle \lambda I^{\rm c}_\lambda \rangle_j\, T^j_{\rm m} W_j + \sum_{i=1,n} \lambda_i I_i T^j_i \right) \tag{4}$$

where $C_{\rm WFC3} = 10^{-8} A_{\rm HST}\,\Omega_{\rm pix}/(hc) = 0.0840241$ counts cm^2 sr erg^{-1} Å^{-1} pixel^{-1} is a constant for the camera, depending on the telescope aperture area, $A_{\rm HST} = \pi(120\ {\rm cm})^2 = 45,239$ cm^2, and the solid-angle subtended[2] by each pixel $\Omega_{\rm pix} = (0.03962'')^2 = 3.6895 \times 10^{-14}$ sr.

We now consider the particular application of deriving a diagnostic ratio between two emission lines: I_1/I_2. It is assumed that observations are made in three filters: Filter I, which targets line 1, Filter II, which targets line 2, and Filter III, which targets the continuum. For optimum results, filters I and II will be narrow-band in order to admit as little continuum as possible, while III will be medium-band so as to efficiently sample the continuum, while at the same time avoiding strong emission lines. However, in practice it is usually impossible to completely avoid emission line contamination of filter III, either by one or both of the target lines (1 and 2), or by other lines that we denote i'. For given line and continuum intensities, I_1, I_2,

[2]Although geometric distorsions by the telescope optics mean that the true pixel area varies across the field of view, this is corrected for during the "drizzle" stage of the pipeline reduction process, which yields images (extension `drz`) interpolated onto a regular pixel grid. If non-drizzled (extension `flt`) images are used, then a further correction for the pixel area map must be applied to equation (4).

Table 1: Filter contamination coefficients, see eq. (11)

Ratio	Filter Set	$\alpha_{\rm I}$	$\alpha_{\rm II}$	$\beta_{\rm I}$	$\beta_{\rm II}$
[N II] 5755/6583	FQ575N, F658N, F547M	0.845	~ 0	0.0243	0.0394
[S II] 6716/6731	FQ672N, FQ674N, F673N	0.994	1.12	0.164	0.114
[S II] 6716/6731	FQ672N, FQ674N, F547M	~ 0	~ 0	0.0274	0.0191
[O III] 4363/5007	FQ437N, F502N, FQ436N	0.968	~ 0	0.711	1.998
[O III] 4363/5007	FQ437N, F502N, F547M	~ 0	0.00141	0.03426	0.09627

Note: Values marked as "~ 0" are all less than 10^{-5}.

$I^{\rm c}_\lambda$, the predicted filter rates are:

$$R_{\rm I} = C_{\rm WFC3}\left[\langle \lambda I^{\rm c}_\lambda\rangle_{\rm I} T^{\rm I}_{\rm m} W_{\rm I} + \lambda_1 I_1 T^{\rm I}_1 + \sum_{i'\neq 1,2} \lambda_{i'} I_{i'} T^{\rm I}_{i'}\right] \tag{5}$$

$$R_{\rm II} = C_{\rm WFC3}\left[\langle \lambda I^{\rm c}_\lambda\rangle_{\rm II} T^{\rm II}_{\rm m} W_{\rm II} + \lambda_2 I_2 T^{\rm II}_2 + \sum_{i'\neq 1,2} \lambda_{i'} I_{i'} T^{\rm II}_{i'}\right] \tag{6}$$

$$R_{\rm III} = C_{\rm WFC3}\left[\langle \lambda I^{\rm c}_\lambda\rangle_{\rm III} T^{\rm III}_{\rm m} W_{\rm III} + \lambda_1 I_1 T^{\rm III}_1 + \lambda_2 I_2 T^{\rm III}_2 + \sum_{i'\neq 1,2} \lambda_{i'} I_{i'} T^{\rm III}_{i'}\right] \tag{7}$$

Note that these equations do not describe the most general case, since they assume that there is negligible contamination of the narrow-band filters by the "other" target line, such that $T^{\rm II}_1 = T^{\rm I}_2 = 0$.[3] The mean continuum intensity in the narrow filters can be related to that in the wider filter by defining color terms:

$$k_{j,\rm III} \equiv \frac{\langle \lambda I^{\rm c}_\lambda\rangle_j}{\langle \lambda I^{\rm c}_\lambda\rangle_{\rm III}} \quad \text{for } j = \text{I, II} \tag{8}$$

The filter color terms can be formally extended to include the contribution of contaminating non-target emission lines:

$$\widetilde{k}_{j,\rm III} \equiv \frac{\langle \lambda I^{\rm c}_\lambda\rangle_j + (T^j_{\rm m} W_j)^{-1}\sum_{i'\neq 1,2}\lambda_{i'} I_{i'} T^j_{i'}}{\langle \lambda I^{\rm c}_\lambda\rangle_{\rm III} + (T^{\rm III}_{\rm m} W_{\rm III})^{-1}\sum_{i'\neq 1,2}\lambda_{i'} I_{i'} T^{\rm III}_{i'}} = k_{j,\rm III}\frac{1+\sum_{i'\neq 1,2} E_{i'}/\widetilde{W}_{j,i'}}{1+\sum_{i'\neq 1,2} E_{i'}/\widetilde{W}_{\rm III,i'}} \tag{9}$$

where the $E_{i'}$ are the equivalent width (in Å) of each non-target line and we have also introduced an "effective width" of each filter with respect to a given emission line:

$$\widetilde{W}_{j,i} \equiv k_{j,i}\frac{T^j_{\rm m}}{T^j_i} W_j \quad \text{with} \quad k_{j,i} \equiv \frac{\langle \lambda I^{\rm c}_\lambda\rangle_j}{\lambda_i I^i_\lambda}. \tag{10}$$

With these definitions, equations (5) to (7) can be solved to give the line ratio in terms of the filter count rates:

$$\frac{I_1}{I_2} = \frac{\lambda_2 T^{\rm II}_2}{\lambda_1 T^{\rm I}_1}\frac{\left[(1-\alpha_{\rm II}\beta_{\rm II}\widetilde{k}_{\rm II,III})R_{\rm I} + \alpha_{\rm II}\beta_{\rm I}\widetilde{k}_{\rm I,III} R_{\rm II} - \beta_{\rm I}\widetilde{k}_{\rm I,III} R_{\rm III}\right]}{\left[\alpha_{\rm I}\beta_{\rm II}\widetilde{k}_{\rm II,III} R_{\rm I} + (1-\alpha_{\rm I}\beta_{\rm I}\widetilde{k}_{\rm I,III})R_{\rm II} - \beta_{\rm II}\widetilde{k}_{\rm II,III} R_{\rm III}\right]} \tag{11}$$

[3] This is a good approximation for the line ratios studied in this paper, but in other cases cannot always be assumed. The general case, which is rather more cumbersome, is treated in Henney et al. (2014).

with filter contamination coefficients

$$\alpha_{\rm I} = \frac{T_1^{\rm III}}{T_1^{\rm I}}; \quad \alpha_{\rm II} = \frac{T_2^{\rm III}}{T_2^{\rm II}}; \quad \beta_{\rm I} = \frac{T_{\rm m}^{\rm I} W_{\rm I}}{T_{\rm m}^{\rm III} W_{\rm III}}; \quad \beta_{\rm II} = \frac{T_{\rm m}^{\rm II} W_{\rm II}}{T_{\rm m}^{\rm III} W_{\rm III}}$$

The α contamination coefficents give the throughput of each target emission line in the continuum filter III relative to the throughput in its respective narrow-band filter, and will tend to be either ~ 1 for lines that fall in the continuum bandpass, or ~ 0 for those that do not. The β contamination coefficients give the integrated continuum throughput in each narrow band filter relative to the continuum filter. Since repeated calibration programs have shown that the WFC3 filter characteristics are stable with time, all these purely instrumental coefficients are constants, albeit with a small systematic uncertainty in their true value. The $\widetilde{k}$ factors, on the other hand, represent the relative strengths of the continuum and non-target lines in the bandpasses of the three filters, and are expected to show variations from object to object and from pixel to pixel within the same object, due to changes in the physical conditions.

1.2. Deriving $T_{\rm e}$, $n_{\rm e}$ from line ratios

1.3. Analysis of fluctuations in $T_{\rm e}$, $n_{\rm e}$

REFERENCES

Brown, T. M. 2006, Filter Throughputs for WFC3 SYNPHOT Support, Instrument Science Report WFC3 2006-3, Space Telescope Science Institute, Baltimore

Henney, W. J., O'Dell, C. R., Ferland, G. J., & Peimbert, M. 2014, In prep

Kalirai, J. S., Baggett, S., Borders, T., & Rajan, A. 2010, The Photometric Performance of WFC3/UVIS: Temporal Stability Through Year 1, Instrument Science Report WFC3 2010-14, Space Telescope Science Institute, Baltimore

Kalirai, J. S., et al. 2009, WFC3 SMOV Proposal 11450: The Photometric Performance and Calibration of WFC3/UVIS, Instrument Science Report WFC3 2009-31, Space Telescope Science Institute, Baltimore

O'Dell, C. R., Ferland, G. J., Henney, W. J., & Peimbert, M. 2013, AJ, 145, 92

Sabbi, E., & the WFC3 Team. 2013, WFC3 Cycle 20 Calibration Program, Instrument Science Report WFC3 2013-05, Space Telescope Science Institute, Baltimore

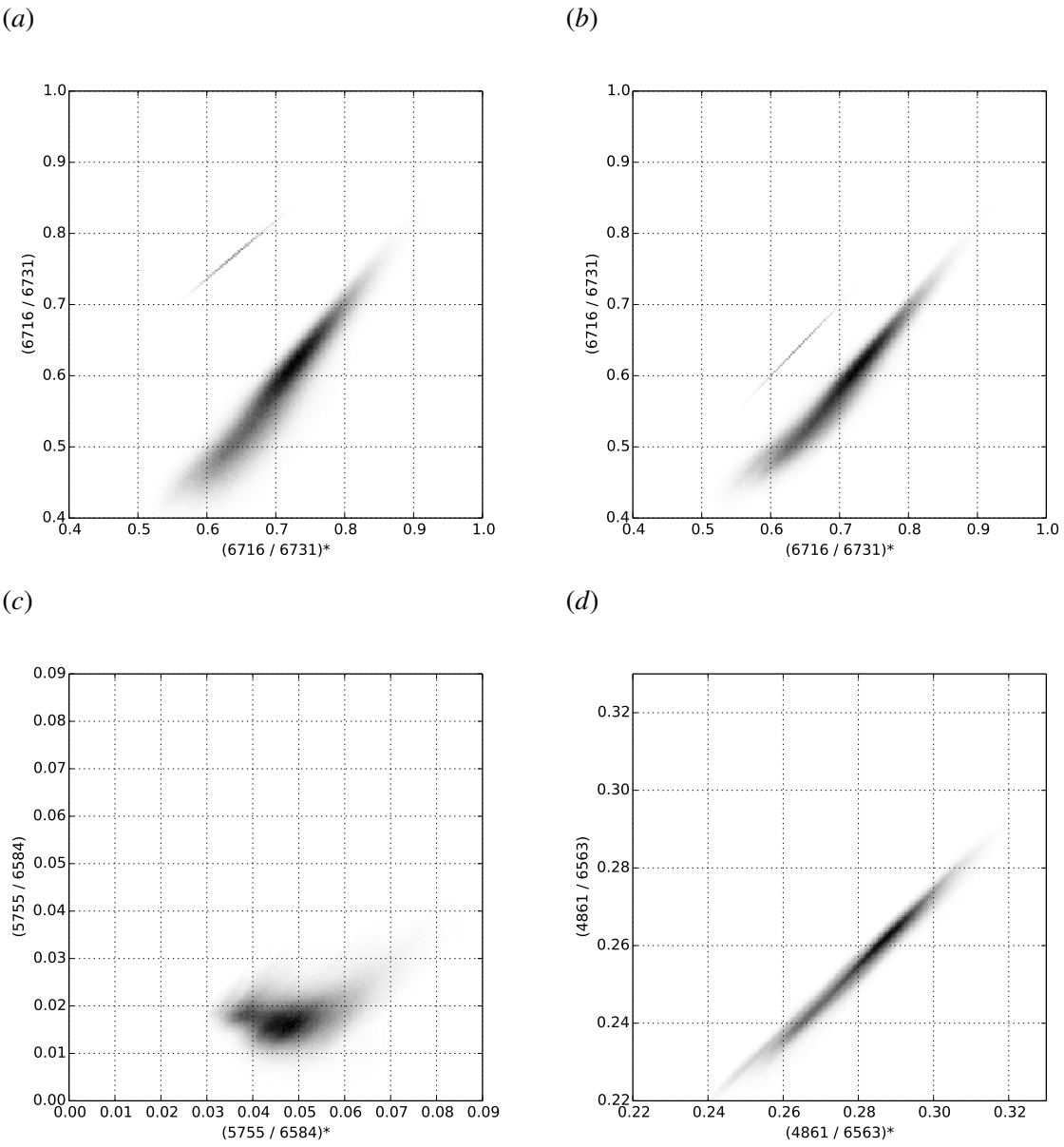

Fig. 1.— Effects on derived line ratios of contamination by continuum and non-target lines. In each panel, the *x* axis shows the "naive" line ratio, while the *y* axis shows the corrected line ratio. (*a*) [S II] 6716/6731 ratio caclulated from FQ672N, FQ674N, F673N; (*b*) [S II] 6716/6731 ratio caclulated from FQ672N, FQ674N, F547M; (*c*) [N II] 5755/6583 ratio caclulated from FQ575N, F658N, F547M; (*d*) Hβ/Hα ratio calculated from F487N, F656N, F547M.